Angle-resolved UV photoemission from Pr(0001)

1992 J. Phys.: Condens. Matter 4 9811

(http://iopscience.iop.org/0953-8984/4/49/009)

J. Phys.: Condens. Matter 4 (1992) 9811–9822. Printed in the UK

Angle-resolved UV photoemission from Pr(0001)

S S Dhesi†, R I R Blyth†, R J Cole†, P A Gravil†, and S D Barrett†‡

† Surface Science Research Centre, University of Liverpool, PO Box 147, Liverpool L69 3BX, UK

‡ Department of Physics, Oliver Lodge Laboratory, University of Liverpool, PO Box 147, Liverpool L69 3BX, UK

Abstract. We have investigated the electronic structure of the rare-earth metal praseodymium using angle-resolved UV photoemission from Pr(0001) and compared the results with band-structure and first-principles photocurrent calculations. Normal-emission valence band spectra in the photon energy range 20–50 eV are dominated by emission from points in the Brillouin zone with a high density of states. The binding energies of the critical points at Γ are found to be 2.5 ± 0.1 eV and 3.6 ± 0.1 eV, in good agreement with bulk band-structure calculations. Off-normal-emission spectra show considerable dispersion and are discussed.

1. Introduction

For a number of years the study of rare-earth metals and rare-earth-based compounds has been an area of considerable scientific endeavour because of the technologically important qualities that they possess. Many of the wide-ranging properties that the rare-earth elements exhibit across the lanthanide series can be attributed directly to the electronic structure of the valence electrons, in particular to the degeneracy that exists between the 5d–6s valence electrons and the 4f states. This structure can be investigated by the well-established method of angle-resolved ultraviolet photoemission (ARUPS) which can probe both the energy (E) and momentum (k) of the electronic states in the valence band [1].

The high reactivity of the rare earths and the resulting difficulties involved in growing single crystals [2] has resulted in a paucity of data with which to test the many band-structure calculations that exist [3, 4]. To date there have been only a few reports of ARUPS on rare-earth single crystals—those published prior to 1992 have been reviewed by Barrett [4]. Of these elements, the most thoroughly investigated is Ho [5], for which the valence band features observed were explained in terms of first-principles one-electron photocurrent calculations. In contrast, only one of the peaks seen on Y(0001) [6] was reproduced by photocurrent calculations employing bulk potentials, indicating the importance of using realistic surface potentials. The most recent report of a rare-earth single-crystal study was the observation of a temperature-dependent conduction-band exchange splitting in ferromagnetic Gd by Kim *et al* [7]. However, there is no attempt to present evidence of a well ordered clean surface in their study—given the difficulties encountered in cleaning rare-earth surfaces [4, 8, 9], this is somewhat surprising.

Irvine *et al* were the first to investigate the electronic structure of Pr using the de Haas–van Alphen effect [10] to study the Fermi surface. Their results were

0953-8984/92/499811+12$07.50

in agreement with calculations for paramagnetic Nd [11], but the topology of the Fermi surface gives no details about the electronic structure at lower energies. In order to gain a better understanding of the electronic structure, we have performed angle-resolved photoemission from the Pr(0001) valence band region and compared the results with first-principles photocurrent calculations employing realistic surface potentials.

Pr has the double *c*-axis hexagonal close packed (DHCP) crystal structure and so its band structure and surface crystal structure differ from those of the hexagonal close packed (HCP) rare earths. The valence band configuration of metallic Pr is ($5d^16s^2$) and it is assumed to have a localised $4f^2$ configuration which is energetically degenerate with the valence band [12]. There has been one reported case of a band-structure calculation for Pr. Fleming *et al* [13] used the relativistic augmented plane wave method to calculate the energy bands and Fermi surface of La, Pr and Nd in order to explain the occurrence of the DHCP structure in the lanthanide series. However, as was the case for many band-structure calculations during the 1960s, it was not self-consistent and we have therefore performed our own band-structure calculations for Pr.

2. Experimental procedure

The Pr sample was spark machined from a high-quality single-crystal boule grown, using zone refining methods [2], by Dr D Fort of the School of Metallurgy and Materials, University of Birmingham, UK. *Ex situ* sample preparation was performed without electropolishing; the mechanically polished surface was not protected by a passivating chloride layer and so the sample was kept under rough vacuum prior to being inserted into the ultra-high vacuum chamber.

The ARUPS experiments were performed on beamline 6.2 of the Synchrotron Radiation Source, at the Science and Engineering Research Council (SERC) Daresbury Laboratory, UK. The spectrometer used was a Vacuum Generators ADES 400 with overall energy and angular resolutions of 0.25 eV and 3° respectively. The base pressure of the chamber was $\sim 3 \times 10^{-10}$ mbar, with the principal residual gas being H. *In situ* sample cleaning involved repeated cycles of Ar^+ bombardment (beam energy $\sim$ 3 keV, current density $\sim$ 10 μA cm^{-2}) and annealing to $\sim$ 650 °C. This cleaning method has been used for many rare earth surfaces [4] and is known to produce clean, well ordered surfaces. Surface cleanliness and order were principally monitored using ARUPS; C and O contamination features appear at $\sim$ 6 eV binding energy and the intensity of the surface-order-dependent state (SODS) at 9.1 eV binding energy is known to be extremely sensitive to the quality of the surface [4]. Approximately thirty cleaning cycles were required before the ARUPS spectra showed a low contamination level and an intense SODS. The sample was kept at 350 °C during data acquisition so that an ARUPS peak observed at a binding energy of $\sim$ 5.5 eV, thought to be derived from H contamination, was kept to a minimum intensity. Low-energy electron diffraction (LEED) showed a sharp (1 × 1) pattern on a low-intensity background [14]. Auger electron spectroscopy showed the level of C contamination to be less than $\sim$ 2% of a monolayer, with no detectable O signal.

3. ARUPS results

A normal-emission spectrum from Pr(0001) taken with p-polarized synchrotron radiation at an energy of 30 eV is shown in figure 1. There are four features below 4 eV, labelled a, b', b and c' in order to maintain the convention adopted for Y [6] and Ho [5]. The valence peaks are at binding energies of 0.3, 1.7, 2.5 and 3.6 eV (all ± 0.1 eV). The SODS, at a binding energy of 9.1 eV, has been observed on HCP rare earths [4–6, 15–17] at a somewhat higher binding energy of $\sim 9.6 \pm 0.2$ eV—the shift in binding energy is due, presumably, to differences in the surface crystal structures between HCP and DHCP metals. There are also contamination-related peaks at ~ 5.5 eV and ~ 6 eV which grew slowly with time and diminished after one cleaning cycle; these have been attributed to H (5.5 eV) and C and O (6 eV). The rising background below ~ 11 eV is due to an $O_{2,3}VV$ Auger transition.

Normal-emission ARUPS spectra of the valence band of Pr(0001), corresponding to emission from states along the ΓA direction of the Brillouin zone, are shown in figure 2. The momentum broadening resulting from the small electron mean free path and the size of the DHCP Brillouin zone along ΓA makes peak dispersion undetectable.

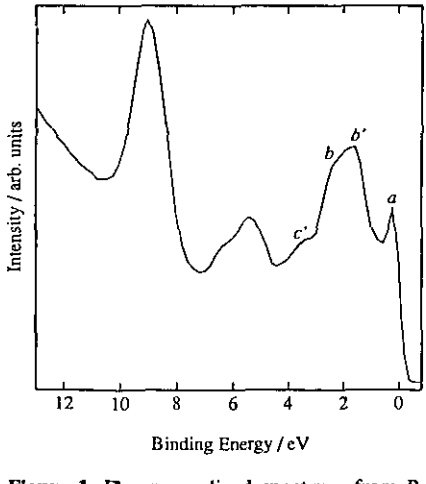

Figure 1. Flux-normalized spectrum from Pr(0001) at normal emission taken using p-polarized synchrotron radiation at an energy of 30 eV. The angle of incidence is 30°.

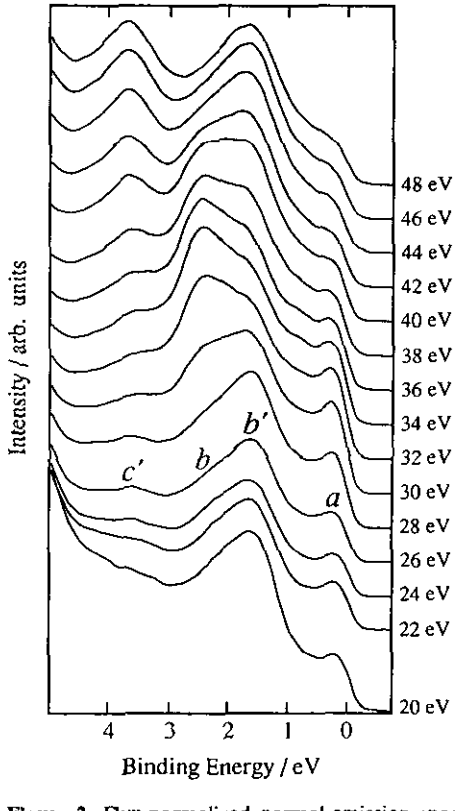

Figure 2. Flux-normalized normal-emission spectra from Pr(0001) over the photon energy range 20–48 eV. The spectra were taken using p-polarized synchrotron radiation at an angle of incidence of 55°.

The intensity of peak a, at a binding energy of 0.3 eV, diminishes with time and increases after a cleaning cycle. A similar peak was observed on the (0001) surfaces of Y [6], Tb [16, 18], Gd [19, 20] and Ho [5] and it was suggested that this peak may originate from a surface state. Since peak a has a similar behaviour to those seen on other rare earths we infer a similar origin.

Off-normal experimental emission spectra from Pr(0001) corresponding to emission from states along the two high-symmetry directions of the surface Brillouin zone, ΓM and ΓKM (figure 3), are shown in figure 4. These spectra effectively show the variation of energy as a function of $k_{\|}$—the dispersion of the valence band features with emission angle can be seen, in marked contrast to the case for normal-emission data. As the electron emission angle is increased from 0°, relative to the surface normal, there is increasing intensity just below the Fermi level. In the case of the ΓKM direction, there are maxima at ~ 24° and around 40–44°, calculated to be emission from the regions of high DOS around the K and M critical points of the Brillouin zone, respectively. In the ΓM direction enhanced features just below the Fermi level are noticeable at +26° and −26°—the negative angle indicates emission on the same side of the surface normal as the incident radiation. This contribution just below the Fermi level is related to emission from regions around the M critical points in two opposite directions from Γ. These features are predicted by the linear muffin-tin orbital (LMTO) band-structure calculation (figure 5) as there are close groupings of bands that develop midway between Γ and both points K and M of the Brillouin zone. For off-normal-emission spectra from Ho(0001) [5] this increase in intensity was also seen along ΓM, but was absent along the ΓKM direction. This was surprising, in that the LMTO calculation showed a tighter grouping of bands along the ΓKM direction than along the ΓM direction. Between 0° and ~ 44°, the spectra along the ΓM direction are symmetrical about ~ 22°. The crystal surface ensures that a movement in either direction from the M critical point is towards a Γ critical point (figure 3). Hence, emission in either direction from the M critical point originates from equivalent points in the Brillouin zone and consequently the spectra will appear to be similar.

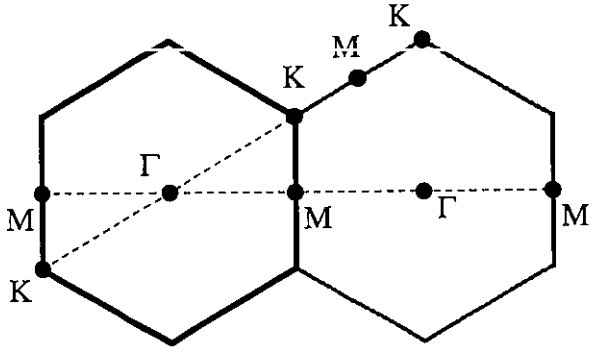

Figure 3. Path of $k_{\|}$ through the Brillouin zone for off-normal emission along ΓM and ΓKM.

Direct comparison of experimental data with calculated band structures has a number of shortcomings. The most notable of these is the use of empirical expressions to determine the component of momentum perpendicular to the surface, $k_{\perp}$, as this is not conserved in the photoemission process. To overcome this we have compared our ARUPS data with first-principles photocurrent calculations in which the initial and final states are calculated explicitly.

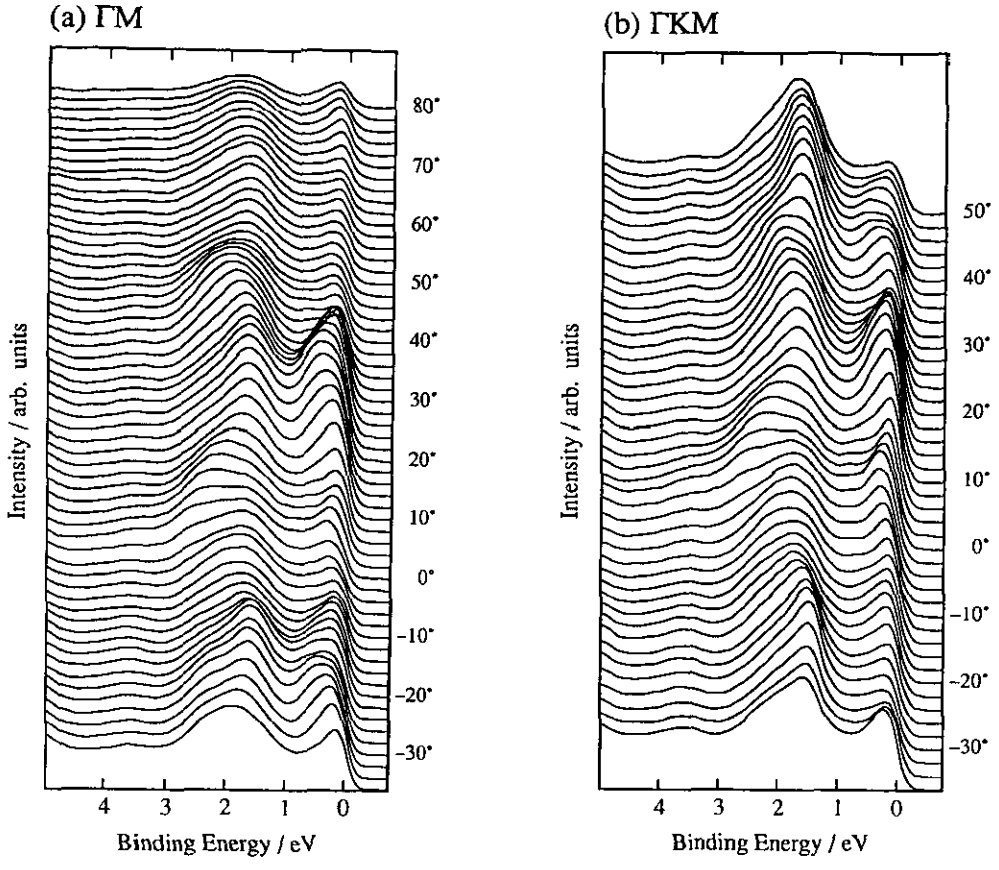

Figure 4. Flux-normalized off-normal-emission spectra from Pr(0001) with the emission angle chosen to vary $k_{\parallel}$ along (*a*) and ΓM and (*b*) the ΓKM direction of the Brillouin zone. Photon energy used was 30 eV, p-polarized radiation incident at 55°.

4. Photocurrent calculations

The calculations were performed on the Cray XMP/48 at the SERC Rutherford Appleton Laboratory, UK, using the (non-relativistic) NEWPOOL code [21]. The potentials were calculated by a self-consistent LMTO 'supercell' method within the atomic sphere approximation (ASA) in which the 4f electrons were treated as core levels. The details of these LMTO calculations have been described elsewhere [5, 22]. For simplicity and speed the supercell was constructed as for an HCP calculation because a DCHP supercell would require more layers in the calculation and hence more computer time. Five layers of Pr atoms were arranged into an ABABA stacking sequence, sandwiched between five layers of vacuum (empty spheres). The calculated potentials from the outer and middle Pr layers were assumed to be representative of the surface and bulk potentials respectively. The NEWPOOL input structure consists of layers of atoms that can be arranged in any sequence with an option to repeat some, or all, or these layers to represent bulk. Hence a DHCP surface can be constructed above a DHCP or an HCP bulk structure. The surface, subsurface and bulk potentials obtained from the LMTO calculation were placed on the top three layers of the

NEWPOOL lattice in order to realistically model the effects of the surface on the photoelectron spectra. The photocurrent calculations were performed for s, p and d orbitals only, i.e., the contribution from the f electrons was not calculated. This was done because the f emission is placed at the wrong energy by NEWPOOL due to the neglect of relaxation effects, thus obscuring valence band detail.

NEWPOOL calculates the probability of an electron being excited from an initial state into a final state for a given set of experimental parameters, i.e. photon energy, polarization, photon angle of incidence and electron angle of emission. As NEWPOOL calculates the initial and final states of the photoelectron explicitly, it can produce band structures for different stacking sequences by varying the structural parameters and the placement of LMTO potentials within the NEWPOOL structure. Hence it can produce the band structures of the surface, subsurface and bulk layers which are useful in the interpretation of the features in the photoemission spectra.

Comparison of the NEWPOOL band structure for 'bulk' potentials from a supercell slab calculation with the LMTO band structure for an infinite crystal gives an indication of the effects of different stacking sequences on the electronic structure. Figure 6 shows a comparison of band structures as calculated by the LMTO method and NEWPOOL using DHCP and HCP bulk stacking sequences. There are twice as many bands when using a DHCP stacking sequence because there are twice as many atoms per unit cell.

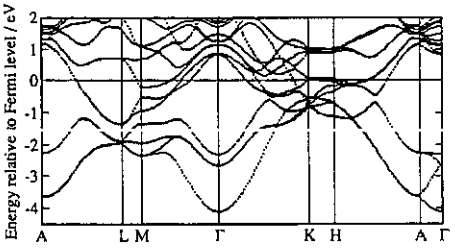

Figure 5. Non-relativistic LMTO band structure for bulk DHCP Pr with the 4f states treated as part of the core.

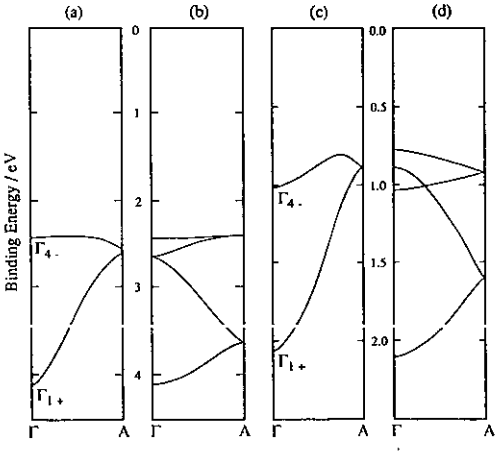

Figure 6. Band structure for Pr along the ΓA direction of the Brillouin zone calculated by (*a*) the LMTO method—HCP stacking, (*b*) the LMTO method—DHCP stacking, (*c*) NEWPOOL—HCP stacking and (*d*) NEWPOOL using a DHCP stacking sequence.

The HCP (0001) surface has two possible terminations (or registries) whereas a DHCP structure has four (figure 7). The first two registries (labelled R1 and R2) have a face centred cubic (FCC)-like stacking sequence in the top three layers, whereas the last two (labelled R3 and R4) have an HCP-like stacking sequence at the surface. The difference in the calculated normal-emission photocurrent spectra using DHCP and HCP bulk stacking sequences with terminations R1 (FCC-like) and R3 (HCP-like)

is negligible (figure 8(*a*) shows the sum of the photocurrents produced by R1 and R3). Surface and subsurface potentials from the LMTO band-structure calculation were placed on the first and second layers of the NEWPOOL structure, with a bulk potential being repeated in the bulk structure. The inverse lifetime of the initial states is normally set to a value that is representative of the experimental peak widths [23]. However, for the spectra in figure 8(*a*) they have been decreased to an artificially low value (reducing the width of the peaks without shifting their positions) in order to exaggerate the difference between the photocurrent spectra from the two different structures.

Common to both spectra are the 1 eV peak and the contribution at ~ 2.0 eV. These are explicable in terms of the band structures calculated by NEWPOOL for the two stacking sequences (figure 6(*c*) and figure 6(*d*)). In the case of the DHCP structure, the 1 eV peak has three closely spaced contributions from the critical points at the top of the Γ band whereas the same peak calculated for the hypothetical HCP structure is derived from the single critical point Γ_{4-}. The broad feature at ~ 2.5 eV is emission from the bottom of the bands at the Γ point. Also shown in figure 8(*a*) is a photocurrent from a NEWPOOL structure that had bulk potentials placed on all layers. The peak just below the Fermi level and the broad feature on the lower binding energy side of the 1 eV peak are absent in this spectrum and thus we conclude that these features are surface related. From the band structure calculated by NEWPOOL using surface potentials (figure 8(*b*)) on all layers, the origins of the broad feature below the 1 eV peak can be deduced. The close grouping of bands around 0.9 eV in the bulk band structure (figure 8(*c*)) is shifted to ~ 1.2 eV in the surface band structure (figure 8(*b*)) and this gives rise to the broad feature below the 1 eV peak.

The two HCP-like terminations produce an identical photocurrent for normal emission, as do the two FCC-like terminations, but for off-normal emission in the $(11\bar{2}0)$ plane the broken symmetry lifts this degeneracy to give unique photocurrent spectra for each termination. The off-normal-emission photocurrent spectra for the four different terminations using in one case a DHCP bulk structure, and in the other an HCP bulk structure, are unique (figure 9(*a*)). When the summation of the photocurrents from the four terminations is convoluted with a Gaussian, to simulate experimental resolution, there appears to be no difference between the spectra obtained using a DHCP bulk structure and that produced using an HCP bulk structure (figure 9(*b*)). Hence, in order to conserve computer time all the calculations were performed using an HCP bulk structure terminated with the four possible DHCP registries. As was the case for previous HCP photocurrent calculations [5], all the terminations were assumed to be equally probable. In contrast to the HCP structure, in which the two terminations are equivalent as far as surface energy considerations are concerned, it is not clear that all four terminations are equivalent for the DHCP structure. However, in the absence of any experimental observations to the contrary (such as could be produced by a quantitative LEED intensity energy study), this was considered to be a reasonable assumption.

5. Discussion of ARUPS results

The photon energy dependence of the calculated normal-emission spectra in the range 20–48 eV is shown in figure 10. All the spectra have been truncated at the Fermi level and convoluted with a Gaussian of FWHM 0.25 eV to simulate the experimental

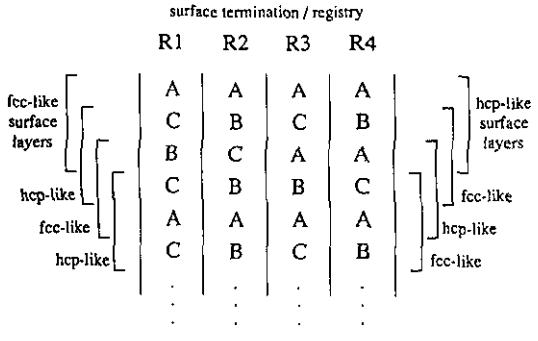

Figure 7. The four possible (0001) terminations of the DHCP structure.

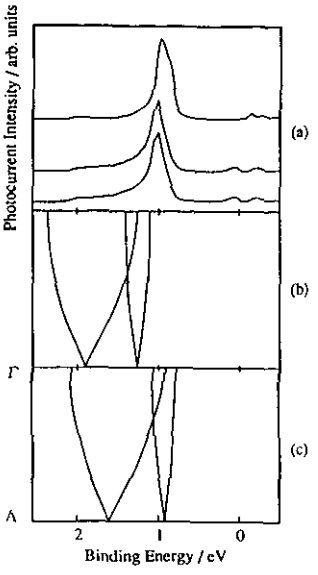

Figure 8. (*a*) Lower spectrum—calculated normal emission spectrum using an HCP bulk stacking sequence; middle spectrum—as for the lower spectrum, but with a DHCP bulk stacking sequence; upper spectrum—as for the middle spectrum, but with bulk potentials used throughout the NEWPOOL structure; (*b*) band structure corresponding to the surface and (*c*) band structure corresponding to the bulk crystal.

resolution. Although NEWPOOL cannot calculate the binding energies of the peaks with absolute precision, the intensity variation exhibited by the experimental peak *b* is well reproduced by the photocurrent peak at a binding energy of 1 eV. We therefore suggest that peak *b* at a binding energy of 2.5 eV originates from the DHCP bulk critical points at the top of the bands at Γ. An LMTO band-structure calculation for hypothetical HCP Pr predicts a binding energy of ~ 2.4 eV for the Γ_{4-} critical point, and the DHCP calculation indicates binding energies of ~ 2.4 eV to ~ 2.6 eV for the three upper critical points at Γ. These values are both in excellent agreement with the value found for peak *b*, but momentum broadening prohibits any clear distinction between the contributions from a DHCP or HCP structure to peak *b*. For other rare-earth metals studied [5, 6, 16, 19, 20] the same peak appears at a similar binding energy, but is lower than the respective LMTO band-structure calculations predict. (Wu *et al* [8, 9] observed a binding energy of 3.6 eV for the Γ_{4-} critical point on Tb—significantly higher than the values found for Y [6], Gd [19, 20], Tb [16] and Ho [5]—probably a consequence of serious Fe contamination.) The intensity of peak *b* increases with increasing p-polarization of incident radiation and this is also correctly calculated by NEWPOOL. Peak *a* is reproduced in the calculation as the surface state just below the Fermi level. The intensity variation of this feature with respect to the incident photon energy does seem to be calculated with a good degree of success (figure 2 and figure 10).

Peak *b'*, at a binding energy of 1.7 eV, is not reproduced in any of the photocurrent calculations. This may be a consequence of using an HCP stacking sequence rather

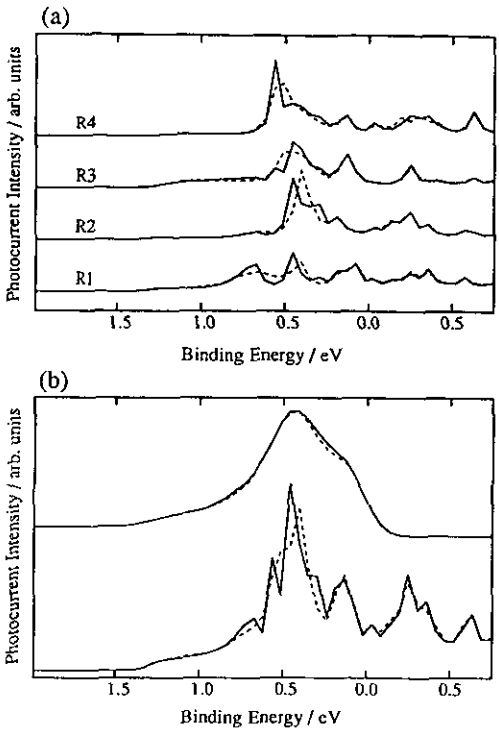

Figure 9. (*a*) Off-normal-emission photocurrent spectra from the four terminations of Pr(0001) using a DHCP bulk (solid line) and an HCP bulk (broken line), along the ΓM direction of the Brillouin zone. The four terminations are labelled according to figure 7. (*b*) The summation of the four off-normal-emission DHCP (solid line) and HCP (broken line) photocurrent spectra in (*a*). The upper spectra have been convoluted with a Gaussian of FWHM of 0.25 eV to simulate the experimental resolution. The photon energy used was 30 eV.

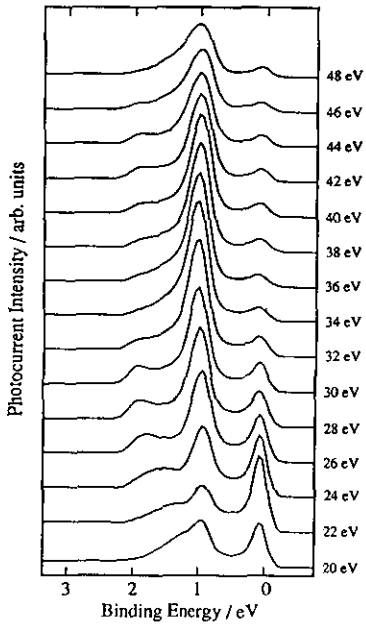

Figure 10. Calculated normal-emission photocurrent spectra in the photon energy range 20–48 eV, p-polarized radiation incident at 55°.

than a DHCP structure in the LMTO band-structure calculation, thus producing inaccurate potentials for the NEWPOOL structure. By analogy to other rare-earth metal studies, peak *b'* was originally assumed to be emission from the critical points at the top of the Γ band. However, the intensity dependence of this peak as a function of photon energy, polarization and electron emission angle is different from that of both peak *b* and the 1 eV photocurrent peak. The peak did not grow with time nor diminish after a clean and its photon energy dependence is different to that found for the common rare-earth contaminating species. Therefore we suggest that it is not a contamination-related peak. An alternative explanation is that it is a many-body feature and consequently not modelled by a one-electron calculation such as NEWPOOL. A study of the neighbouring element Nd, which also has the DHCP structure, could be useful in determining its origin.

Peak c' at a binding energy of 3.6 eV was thought to be simply 4f related emission since the binding energy is in good agreement with the x-ray photoemission work of Lang *et al* [24]. However, the intensity of this peak does not increase monotonically with photon energy in the range 20–50 eV, in contrast to the cross section for 4f electrons as calculated by Yeh and Lindau [25], and hence we deduce that there is an additional contribution present. The photon energy dependence of the intensity of the background-subtracted peak c', together with the intensity of the 2.1 eV photocurrent peak, is shown in figure 11. From the good agreement we can infer that there is a contribution to peak c' from the bottom of the bands at the Γ critical point. An LMTO band-structure calculation for Pr predicts a value of ~ 4.1 eV for this point (figure 5).

Figure 11. *Photon energy dependence of* experimental peak c (●) and the calculated photocurrent peak at 1.75 eV (○).

Calculated off-normal-emission spectra with the electron emission angle chosen to vary $k_{\parallel}$ along the ΓM and ΓKM directions of the Brillouin zone are shown in figure 12. Comparison with the experimental spectra (figure 4) shows that the dispersion of peak b towards the Fermi level between 0° and $\sim 10°$ is reproduced by the 1 eV photocurrent peak. The increase in intensity just below the Fermi level along the ΓM direction of the Brillouin zone is correctly calculated by NEWPOOL. However, this is not the case along the ΓKM direction where there is no enhanced contribution at the Fermi level. The photocurrent spectra in the ΓM direction (figure 12(a)), between $\sim 10°$ and $\sim 24°$ (the M point), show a feature that disperses back towards higher binding energy from ~ 1 eV to ~ 1.5 eV. In contrast, the photoemission data along the ΓM direction (figure 4(a)) show that peak b disperses monotonically towards lower binding energy between $\sim 0°$ and $\sim 22°$. A possible explanation for this discrepancy could be that NEWPOOL is inaccurately calculating the band structure in this direction of the Brillouin zone. However, this is unlikely because of the success that it has in predicting the dispersion of peak b in the ΓKM direction (figure 4(b) and figure 12(b)).

The photocurrent peak at a binding energy of ~ 2.1 eV for normal emission also disperses towards the Fermi level between 0° and $\sim 10°$. However, the low intensity of this peak, together with the 4f contribution to the experimental spectra makes the detection of this feature rather difficult.

6. Summary

We have identified most of the peaks in the valence band of Pr(0001) and determined

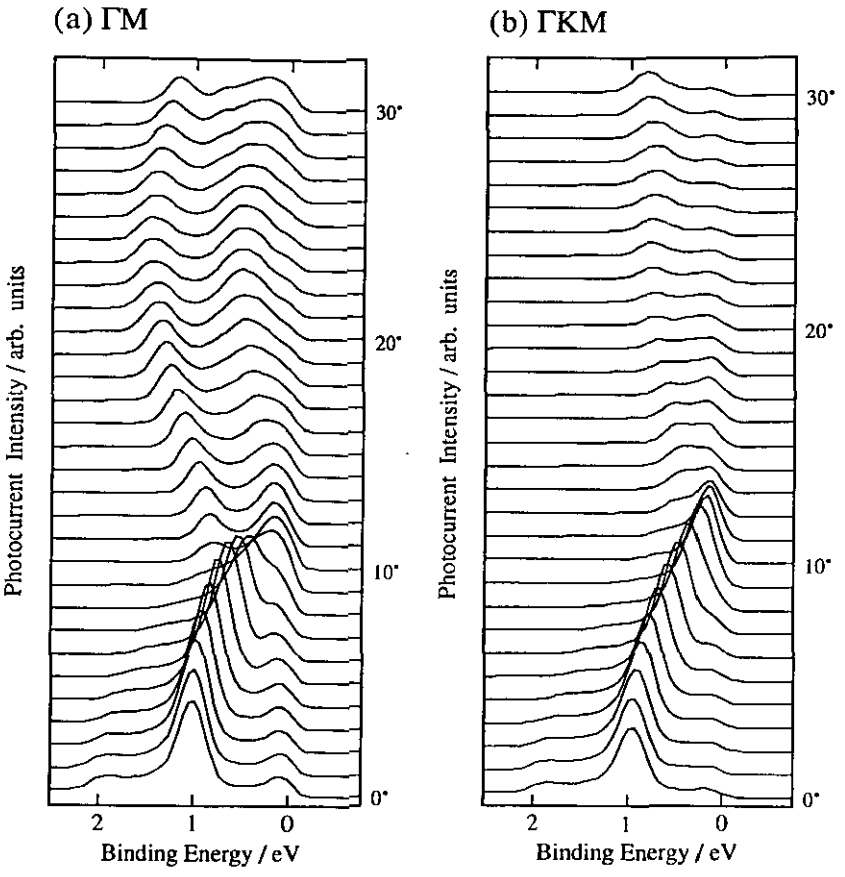

Figure 12. Calculated off-normal-emission photocurrent spectra with the emission angle chosen to vary $k_{\parallel}$ along (*a*) the ΓM and (*b*) the ΓKM direction of the Brillouin zone. The photon energy used was 30 eV, p-polarized radiation incident at 55°.

their origins by comparison with first-principles photocurrent calculations. By analogy to the study of the (0001) surfaces of other rare-earth metals and photocurrent calculations for Pr(0001), peak *a* is assigned to a surface state lying just below the Fermi level. Peak *b*, at a binding energy of 2.5 ± 0.1 eV, is emission from regions of high DOS at the top of the bands at Γ. Peak *c'*, at a binding energy of 3.6 ± 0.1 eV, is a 4f emission peak with a contribution from the bottom of the bands at Γ. These peaks are well modelled by photocurrent calculations, but the binding energies are low in comparison with experimental studies. A possible explanation is that we have used an HCP supercell in our initial LMTO–ASA band-structure calculation and the resultant layer potentials are not representative of the DHCP structure. In addition, the interaction of the photoelectron with the hole it creates (the relaxation energy) is neglected and consequently the calculated binding energies of the peaks are affected. Peak *b'* in the experimental spectra is not reproduced in the photocurrent calculations. A study of the neighbouring element Nd, which has the same DHCP structure, could be useful in determining the origin of this peak and confirming the identification of others. With the exception of peak *b'*, comparison with NEWPOOL has enabled peaks in the valence band photoemission spectrum to be identified. Quantitative

LEED analysis is needed to determine the actual surface structure of Pr(0001), as our assumptions concerning the surface geometry may be invalid. This is being undertaken in order to refine our photocurrent calculations.

Acknowledgments

We would like to thank Dr David Fort (School of Metallurgy and Materials, University of Birmingham) for growing the high-quality rare-earth single crystal. Dr Tracy Turner, the rest of the SRS support staff (Daresbury Laboratory) and Buck Dharma are acknowledged for assistance during data acquisition. Dr Tony Begley (SUNY, USA) is thanked for performing the LMTO–ASA slab calculations as is Dr Richard Blake (Daresbury Laboratory) for many useful discussions. Martin Evans is thanked for assistance with the photocurrent calculations. SSD, RIRB, RJC and PAG acknowledge receipt of SERC studentships. This work was funded by the SERC and we are grateful for their support.

References

[1] See, for instance,
Smith N V 1978 *Photoemission from Solids I: General Principles* ed M Cardona and L Ley (Berlin: Springer) ch 6
[2] Fort D 1989 *J. Cryst. Growth* **94** 85
[3] Liu S H 1978 *Handbook on Physics and Chemistry of Rare Earths* vol 1, ed K A Gschneidner Jr and L Eyring (Amsterdam: North-Holland) p 233
[4] Barrett S D 1992 *Surf. Sci.* **14** 271
[5] Blyth R I R, Barrett S D, Dhesi S S, Cosso R, Heritage N, Begley A M and Jordan R G 1991 *Phys. Rev.* B **44** 5423
[6] Barrett S D and Jordan R G 1987 *Z. Phys.* B **66** 375
[7] Kim B, Andrews A B, Erskine J L, Kim K J and Harmon B N 1992 *Phys. Rev. Lett.* B **68** 1931
[8] Wu S C, Li H, Tian D, Quinn J, Li Y S, Jona F, Sokolov J and Christensen N E 1990 *Phys. Rev.* B **41** 11 911
[9] Wu S C, Li H, Tian D, Quinn J, Li Y S, Jona F, Solokov J and Christensen N E 1991 *Phys. Rev.* B **43** 12 060
[10] Irvine S J C, Young R C, Fort D and Jones D W 1978 *J. Phys. F: Met. Phys.* **8** L269
[11] Fleming G S, Liu S H and Loucks T L 1969 *J. Appl. Phys.* **40** 1285
[12] Wieliczka D M and Olson C G 1984 *Phys. Rev. Lett.* **52** 2180
Szotek Z, Temmerman W M and Winter H 1991 *Physica* B **172** 19
[13] Fleming G S, Liu S H and Loucks T L 1968 *Phys. Rev. Lett.* **21** 1524
[14] Blyth R I R, Cosso R, Dhesi S S, Newstead K, Begley A M, Jordan R G and Barrett S D 1991 *Surf. Sci* **251/252** 722
[15] Blyth R I R, Dhesi S S, Gravil P A, Newstead K, Cosso R, Cole R J, Patchett A J, Mitrelias T, Prince N P and Barrett S D 1992 *J. Alloys Compounds* **180** 259
[16] Blyth R I R, Patchett A J, Dhesi S S, Mitrelias T, Prince N P and Barrett S D 1991 *J. Phys.: Condens. Matter* **3** 6165
[17] Barrett S D, Blyth R I R, Begley A M, Dhesi S S and Jordan R G 1991 *Phys. Rev.* B **43** 4573
[18] Wu S C, Li H, Li Y S, Tian D, Quinn J, Jona F and Fort D 1991 *Phys. Rev.* B **44** 13 720
[19] Himpsel F J and Reihl B 1983 *Phys. Rev.* B **28** 574
[20] Jordan R G 1986 *Phys. Scr.* T **13** 22
[21] Larsson C G 1985 *Surf. Sci.* **152/153** 213
[22] Begley A M, Jordan R G, Temmerman W M and Durham P J 1990 *Phys. Rev.* B **41** 11 780
[23] Barrett S D, Begley A M, Durham P J and Jordan R G 1989 *Solid State Commun.* **71** 111
[24] Lang J K, Baer Y and Cox P A 1981 *J. Phys. F: Met. Phys.* **11** 121
[25] Yeh J J and Lindau I 1985 *At. Data Nucl. Data Tables* **32** 1